









RESEARCH ARTICLE | APRIL 01 2022

A concept of a broadband inverted geometry spectrometer for the Second Target Station at the Spallation Neutron Source

Special Collection: [New Science Opportunities at the Spallation Neutron Source Second Target Station](#)

E. Mamontov ; C. Boone ; M. J. Frost ; K. W. Herwig ; T. Huegle ; J. Y. Y. Lin ; B. McCormick; W. McHargue; A. D. Stoica; P. Torres ; W. Turner 

 Check for updates

Rev. Sci. Instrum. 93, 045101 (2022)

<https://doi.org/10.1063/5.0086451>


View
Online


Export
Citation



APL Energy

Latest Articles Online!

Read Now

A concept of a broadband inverted geometry spectrometer for the Second Target Station at the Spallation Neutron Source

Cite as: Rev. Sci. Instrum. 93, 045101 (2022); doi: 10.1063/5.0086451

Submitted: 25 January 2022 • Accepted: 11 March 2022 •

Published Online: 1 April 2022



View Online



Export Citation



CrossMark

E. Mamontov,^{1,a)} C. Boone,² M. J. Frost,³ K. W. Herwig,² T. Huegle,³ J. Y. Y. Lin² B. McCormick,² W. McHargue,³ A. D. Stoica,¹ P. Torres,² and W. Turner²

AFFILIATIONS

¹Neutron Scattering Division, Oak Ridge National Laboratory, Oak Ridge, Tennessee 37831, USA

²SNS Second Target Station Project, Oak Ridge National Laboratory, Oak Ridge, Tennessee 37831, USA

³Neutron Technologies Division, Oak Ridge National Laboratory, Oak Ridge, Tennessee 37831, USA

Note: Paper published as part of the Special Topic on New Science Opportunities at the Spallation Neutron Source Second Target Station.

^{a)}Author to whom correspondence should be addressed: mamontove@ornl.gov. Tel.: 1-865-771-1387. Fax: 1-865-574-6080

ABSTRACT

BWAVES is an acronym for Broadband Wide-Angle VELOCITY Selector spectrometer, indicating that a novel WAVES (Wide-Angle VELOCITY Selector) device will be used to select the velocity/wavelength of the detected neutrons after they are scattered by the sample. We describe a conceptual design of BWAVES, a time-of-flight broadband inverted-geometry neutron spectrometer for the Second Target Station at the Spallation Neutron Source operated by Oak Ridge National Laboratory. Being the first inverted geometry spectrometer where the energy of the detected neutrons can be chosen by a WAVES device mechanically, irrespective of the limitations imposed by the crystal analyzers or filters, BWAVES will feature a uniquely broad, continuous dynamic range of measurable energy transfers, spanning 4.5 decades. This will enable measurements of both vibrational and relaxational excitations within the same, continuous scattering spectra. Novel approaches that are necessary for the implementation of a WAVES device at the BWAVES spectrometer will result in a spectrometer with the design and characteristics much different from those displayed by the neutron spectrometers in existence today.

© 2022 Author(s). All article content, except where otherwise noted, is licensed under a Creative Commons Attribution (CC BY) license (<http://creativecommons.org/licenses/by/4.0/>). <https://doi.org/10.1063/5.0086451>

I. INTRODUCTION

Inverted geometry neutron spectrometers select a fixed “final” energy, E_f , of the detected neutrons after they are scattered by a sample. The energy transfer between a neutron and the sample, $E = E_i - E_f$, is calculated by determining the “initial” neutron energy, E_i , usually via measuring the neutron time-of-flight (TOF). The important features of the inverted geometry neutron spectrometers are (1) the highest energy resolution achievable at the elastic line, where $E = 0$, and (2) access to the broad range of the energy transfers with $E > 0$ even at low temperatures, where, because of the low Bose population factor, the probability of neutron up-scattering by the sample (neutron gaining energy) is low. The former feature is often used advantageously in high energy-resolution backscattering spectrometers optimized for quasi-elastic neutron scattering (QENS)

measurements at low values of E . The latter feature is utilized in inelastic neutron scattering (INS) measurements at vibrational spectrometers. While the QENS-dedicated backscattering spectrometers feature a high energy-resolution to enable measurements at low E , they tend to suffer from the limited range of accessible energy transfers, in the hundredths of meV for the classic reactor-based^{1,2} and tenths of meV or at best \sim meV for the TOF reactor- or spallation source-based^{3–9} backscattering spectrometers. This complicates studies of broad multi-component relaxational dynamics, which is especially characteristic of biological and soft matter samples, but also present in many complex chemical systems. On the other hand, even the two vibrational spectrometers with the widest range of the accessible energy transfers in operation today^{10,11} achieve an energy resolution somewhat above 0.1 meV at the elastic line and, as molecular spectroscopy-dedicated instruments, lack the

scattering momentum transfer ($Q = k_i - k_f$) coverage, having analyzer banks positioned only at two scattering angles (45° and 135°). This is inconvenient for studying samples that exhibit, besides the INS signal, diffusion or relaxation-type dynamics giving rise to the QENS signal.

Our goal is to design and build a broadband inverted geometry spectrometer with a high energy resolution for the Second Target Station (STS) at the Spallation Neutron Source (SNS) for QENS and INS measurements. From the QENS measurements standpoint, the broadband designation refers to a QENS-capable spectrometer with the dynamic range so wide that no dynamics of quasielastic origin, no matter how broad a signal it gives rise to, would be missing from the measured spectra. That is, the extension of the QENS dynamic range is to be achieved by increasing the energy transfer range compared to that presently available at the QENS-capable spectrometers, thus enabling thorough analysis of broad multi-component relaxation dynamics. From the INS measurements standpoint, the broadband designation refers to a vibrational spectrometer with the greatly improved energy resolution at the elastic line compared to the best vibrational spectrometers in operation today, which will enable measurements of the diffusion and relaxational dynamics in the samples besides the vibrational dynamics. That is, the extension of the INS dynamic range is to be achieved by decreasing the measurable energy transfers (via improving the energy resolution at the elastic line) compared to that presently available at the world's best vibrational spectrometers.

This paper concentrates specifically on the design and parameters of a broadband inverted geometry spectrometer with a high energy resolution for the SNS Second Target Station.

II. GENERAL CONSIDERATION FOR THE SPECTROMETER LAYOUT

Besides the requirement for a broadband high-energy resolution spectrometer for simultaneous studies of vibrations and relaxations, a highly focused incident neutron beam, making possible studies of small samples, could be of significant importance. First, it would allow studies of samples available in small quantities, such as hard to make or hard to deuterate selectively bio-, soft, and chemical samples. Second, it would be compatible with advanced sample environments, e.g., pressure cells, which typically can utilize only a limited sample volume.

Based on the extensive experience of studies of complex systems using neutron spectrometers such as TOSCA, IRIS, OSIRIS (Rutherford Appleton Laboratory, UK), BASIS, and VISION (Oak Ridge National Laboratory, USA), the high-level requirements for the spectrometer we consider can be formulated as presented in Table I. Studies of relaxations in soft- and bio-systems require an energy resolution comparable to the Pyrolytic Graphite 002 reflection option at IRIS or OSIRIS (0.0175–0.0254 meV, FWHM) or silicon (311) reflection option at BASIS (0.0150 meV, FWHM). Concurrently, the energy transfer range should greatly exceed that of Pyrolytic Graphite 002 reflection option at IRIS or OSIRIS (0.4 meV) or silicon (311) reflection option at BASIS (0.66 meV) and be comparable with that at TOSCA and VISION. To target relaxations in complex systems, an extension of the minimal Q below the currently achievable at BASIS value of 0.3 \AA^{-1} might be desirable, whereas the Q -resolution could be similar to, or somewhat more relaxed

TABLE I. High-level requirements for a broadband neutron spectrometer for the SNS STS.

Neutron beam size	$\sim 5 \times 5 \text{ mm}^2$
Energy resolution at the elastic line	$\sim 0.020 \text{ meV}$, FWHM
Energy transfer	$\geq 500 \text{ meV}$
Minimum momentum transfer at the elastic line	$\leq 0.3 \text{ \AA}^{-1}$
Momentum transfer resolution at the elastic line	$\sim 0.1 \text{ \AA}^{-1}$

compared to the BASIS value of $0.05\text{--}0.10 \text{ \AA}^{-1}$. Finally, to target a sample volume of a few microliters, for a typical hydrogenous sample of $\sim 0.1 \text{ mm}$ thickness (to control multiple scattering effects), a $5 \times 5 \text{ mm}^2$ incident beam would be commensurate with $\sim 2.5 \mu\text{l}$ sample volume.

Design of a spectrometer with such characteristics is challenging. We start with the general consideration, as follows:

1. We aim at collecting the entire scattering spectrum within one neutron pulse timeframe of 0.066667 s from a proton pulse on the target, as defined by the source repetition rate of 15 Hz . This is important in order to (1) ensure that the background counts from thermalized neutrons that cannot be completely suppressed change monotonically as a function of the energy transfer (that is, TOF) within the spectrum and (2) avoid having to splice together multiple spectra with the dynamic components possibly extending across the boundaries of the spectra.
2. Moreover, because the spectrum is to include the highest energy transfer data associated with the TOF values close to zero, similar to the existing neutron vibrational spectrometers,^{10,11} the measurement of the entire scattering spectrum needs to be completed within, specifically, the first neutron pulse timeframe, that is, between 0 and 0.066667 s , as opposed to, e.g., between 0.066667 and 0.133333 s , from a given proton pulse on the target.
3. Because simultaneous arrival to the sample position of the slowest incident neutrons from a pulse with the fastest incident neutrons from the next pulse is to be avoided to discriminate between detecting neutrons from different pulses, the spectrometer's primary flight path, from the moderator to the sample position, needs to be as short as practical.
4. Likewise, from the background considerations, the collection of the slowest neutrons from a pulse scattered by the sample needs to be fully completed before the next pulse. That is, such slowest neutrons need to arrive before the next pulse not merely to the sample position, but the detectors, thus dictating that the spectrometer's secondary flight path, from the sample position to the detectors, also be short.
5. Besides these practical considerations, the vacuum detector vessel of a spectrometer with a short primary flight path must be sufficiently compact anyway in order to fit between the structures of the neighboring beam lines.
6. A pulse-shaping chopper is not to be used for the incident neutrons, because it would inevitably restrict the accessible range

of the energy transfers. Then, assuming the overall energy resolution of the spectrometer $\delta E = (\delta E_p^2 + \delta E_s^2)^{1/2}$, where δE_p and δE_s is the contribution from the primary and secondary flight path, respectively, the δE_p is already limited by the pulse width of the moderator for the elastic line wavelength ($E_i = E_f$). In the first approximation, this pulse width is the main contribution to the time-of-flight uncertainty due to the primary flight path, δTOF , and $\delta E_p = 2E_p(\delta \text{TOF}/\text{TOF})$. Therefore, a choice of a long neutron wavelength for the elastic line (a low E_f) can reduce δE_p by means of reducing E_p and increasing TOF, while the moderator pulse width, largely defining δTOF , tends to plateau for the long wavelength neutrons.

- The traditional way to select the elastic line neutron wavelength at the inverted geometry spectrometers (that is, λ_f , E_f) is by using Bragg reflection from the analyzer crystals. For long wavelengths ($\lambda_f > 7 \text{ \AA}$), the choice of suitable analyzer crystal is limited, perhaps, to mica (002) reflection only. However, there would be no suitable materials for filtering out the higher order mica reflections, such as (004), (006), etc. To this end, a long λ_f will need to be selected mechanically, by a novel WAVES (Wide-Angle VELOCITY Selector) device.^{12–15}
- Efficient use of a WAVES device requires a small sample,^{12,15} as will be discussed in more detail below. Moreover, unless only a narrow incident neutron bandwidth is intended to be selected by a WAVES device,^{13,15} the access of the incident neutron beam to the sample position at a broadband spectrometer requires an open geometry, with only one hemisphere (typically, the bottom) occupied by a WAVES device and an unobstructed horizontal plane where the sample is positioned.

Therefore, we need to design a short neutron spectrometer with a compact vacuum detector vessel and an open tabletop geometry to collect the very broadband wavelength scattering spectra in a single neutron pulse frame using a WAVES device to mechanically select the “final” wavelength (which is also the elastic line wavelength) of the detected neutrons after they are scattered by the sample.

Within the limitations of the allocated floor space at beamline 7 of the SNS STS, a conceptual design of BWAVES (which is an acronym for Broadband Wide-Angle VELOCITY Selector) spectrometer achieves single-frame operation as illustrated in Fig. 1 using the primary (moderator to sample) flightpath $L_p = 14.65 \text{ m}$ and the secondary (sample to detectors) flight path $L_f = 0.35 \text{ m}$ (on average) with the longest measured wavelength $\lambda_{\text{max}} = 17.44 \text{ \AA}$ as presented by the lines of the minimum slope ($v_{\text{min}} = 226.8 \text{ m/s}$, $E_{\text{min}} = 0.269 \text{ meV}$) in Fig. 1. Choosing $\lambda_f = \lambda_{\text{elastic}} = 14.50 \text{ \AA}$, as represented by the lines of the slightly higher slope ($v_f = 272.8 \text{ m/s}$, $E_f = 0.389 \text{ meV}$) in Fig. 1, allows for neutron detection at the negative energy transfers, $E = E_i - E_f$, of up to -0.120 meV , as necessary for the resolution function measurements at the elastic line.

III. SPECTROMETER COMPONENTS

A. Neutron choppers

The short primary flight path simplifies the design of the choppers for the BWAVES spectrometer. A bandwidth selection chopper, defining the wavelength range of the incident neutrons, could be

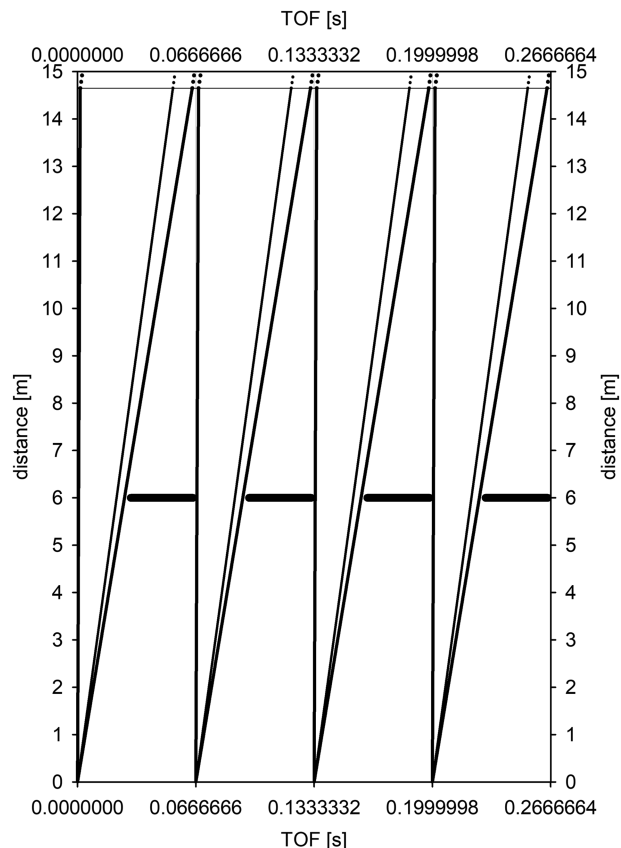


FIG. 1. The BWAVES spectrometer timing diagram showing the default operation mode measuring the scattering spectrum within one neutron pulse time frame. A single bandwidth selection chopper at 6 m from the moderator eliminates $17.44 < \lambda < 43.95 \text{ \AA}$ incident neutrons (not shown is a T0 chopper at 9.25 m from the moderator for the suppression of the gamma-rays and fast neutrons associated with the prompt pulse).

positioned anywhere between the moderator and the sample, as allowed by the geometry of the bunker. However, a chopper positioned as close to the moderator as possible increases the minimal wavelength at which neutron leakage through the chopper starts. With a position at 6 m from the moderator, as shown in Fig. 1, the chopper eliminates $17.44 < \lambda < 43.95 \text{ \AA}$ incident neutrons. At this position, a disk chopper for bandwidth selection spinning at 15 Hz will have an opening of 143° .

A T0 chopper is necessary for the suppression of the gamma-rays and fast neutrons associated with the prompt pulse. At the same time, the design and placement of a T0 chopper define the shortest neutron wavelength transmitted without getting blocked by the chopper. For a T0 chopper positioned at 9.25 m from the moderator and spinning at 15 Hz, assuming $3 \times 3 \text{ cm}^2$ incident beam (commensurate with the moderator size) and 1.24 m rotor diameter, the minimum wavelength transmitted to the sample not being blocked by the chopper is $\lambda_{\text{min}} = 0.23 \text{ \AA}$ ($v_{\text{max}} = 171\,97.8 \text{ m/s}$, $E_{\text{max}} = 1546 \text{ meV}$).

B. Neutron guide

The BWAVES neutron guide is supposed to focus an incident neutron beam from the $3 \times 3 \text{ cm}^2$ moderator to the sample of a size $5 \times 5 \text{ mm}^2$ (the sample size limitations will be further discussed in Sec. III C). A supermirror ($m = 6$) neutron guide extends from a distance of 1 m from the moderator to 13.78 m from the moderator (0.87 m to the sample position). A supermirror with $m = 6$ as a maximum is the best choice that is practical at present from the standpoint of the reflectivity and cost. The guide's horizontal and vertical cross sections are the same. The guide consists of two elliptical sections, one spanning 1–9 m, another 9.50–13.78 m, from the moderator (Fig. 2). The T0 chopper, centered at 9.25 m from the moderator, is accommodated in the 0.50 m gap between the two guide sections. It should be noted that a minimally required 0.30 m thickness of the T0 chopper necessitates a minimum gap of at least 0.45 m between the upstream and downstream guide sections. The guide provides a beam divergence at the sample position of $\sim 1.5^\circ$ (full width at half maximum) in both horizontal and vertical directions.

The theoretical wavelength-dependent critical neutron reflection angle for $m = 6$ supermirror is $0.00173 \times \text{m rad}/\text{\AA} = 0.01 \text{ rad}/\text{\AA}$, and the BWAVES guide system transmits neutrons with minimum losses up to the shortest wavelength of $\sim 2.5 \text{ \AA}$. The latter point can be illustrated by the calculation presented in Fig. 3, where, as a function of incident wavelength, we plot brilliance transfer, a dimensionless factor that is calculated as a ratio of neutron spectrum on the sample to a product of brilliance of the source, size of the sample, and beam divergence on the sample. The reflectivity-limited drop in the brilliance transfer is evident for the wavelengths shorter than $\sim 2.5 \text{ \AA}$.

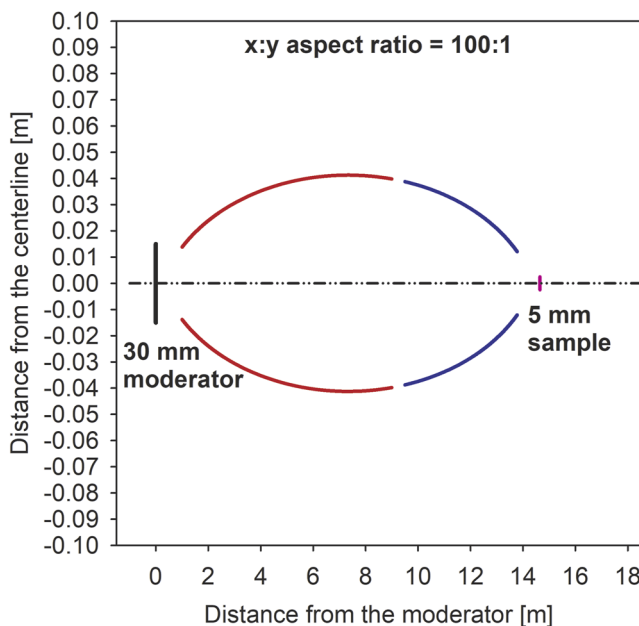


FIG. 2. The two elliptical guide sections (shown in red and blue) of the BWAVES spectrometer. The gap accommodates the T0 chopper at 9.25 m from the moderator. The guide's horizontal and vertical cross sections are the same.

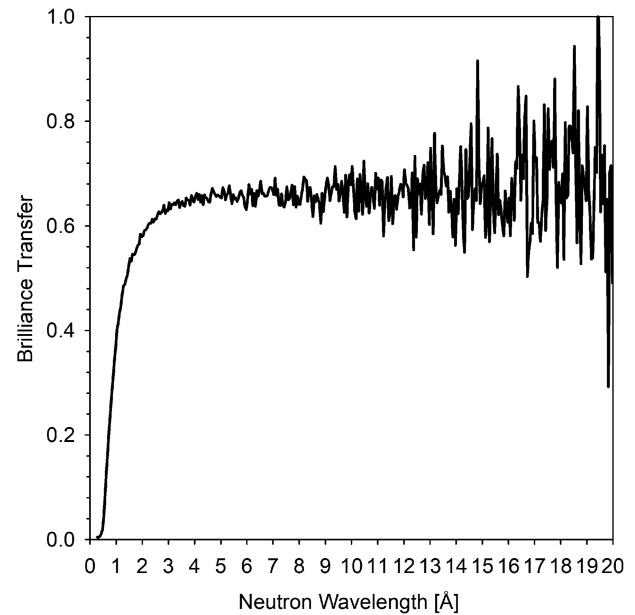


FIG. 3. The brilliance transfer, $BT = \text{Spectrum}(\text{sample})/[\text{Brilliance}(\text{source}) * \text{size}(\text{sample}) * \text{divergence}(\text{sample})]$, calculated for the BWAVES spectrometer for a $5 \times 5 \text{ mm}^2$ spot at the sample position.

C. WAVES rotor

As the device for selection of the final neutron velocity, v_f (wavelength, λ_f), the WAVES rotor is the most critical component of the BWAVES spectrometer. For infinitely thin blades and a point sample, the analytical expression for the energy resolution of the WAVES device (FWHM) is^{12,13} $\Delta E_f = 2E_f[v_f/n_b f(R_{\text{max}} - R_{\text{min}})] = 2E_f(360^\circ A/n_b(R_{\text{max}} - R_{\text{min}}))$, where n_b is the number of the Archimedean spiral-shaped neutron adsorption blades extending from R_{min} to R_{max} , f is the frequency of the device rotation, and E_f and v_f are the energy and velocity of the neutrons to be passed by the selector, according to the designed blades curvature that is described by an equation in the polar coordinates $r = A\phi$, with $A = v_f/(360^\circ f)$. From the standpoint of the spectrometer operation, for a given WAVES rotor with a blade shape of $r = A\phi$, a longer transmission wavelength, resulting in the finer energy resolution, can be readily chosen by lowering the rotation frequency and, therefore, the transmitted neutron velocity, because the blade curvature is fixed by design at $A = v_f/(360^\circ f)$; thus, v_f is proportional to f . On the other hand, a shorter transmission wavelength could not be chosen readily, as this would require increasing f (to increase v_f) beyond the limit imposed by the structural stability of the rotor. A WAVES rotor could be designed and built for any chosen value of λ_f (that is, v_f) at the maximum allowed f , not necessarily specifically for $\lambda_f = 14.50 \text{ \AA}$ as chosen for the current BWAVES design. However, from the operational standpoint, the spectrometer's λ_f , whether of 14.50 \AA or any other value, could be readily increased (leading to a finer energy resolution in the optional “booster” mode as described below), but not decreased, unless the WAVES rotor utilized at the spectrometer is replaced by another rotor with a different blade curvature.

Besides the assumption of the infinitely thin blades and a point sample, the analytical expression given above was derived for two-dimensional geometry of neutrons passing through the WAVES device after been scattered by a sample in the horizontal plane where the sample is positioned. For a neutron scattered by the sample with a finite vertical scattering angle component, α (out of the horizontal plane), the horizontal velocity component is modulated by $\cos \alpha$. Thus, for a WAVES device with straight vertical blades of the shape described by $r = \varphi v_f / (360^\circ f)$, a neutron scattered by the sample needs to have a total velocity of $v_f / \cos \alpha$ to be transmitted.

Figure 4 shows the calculated transmission, which is analogous to the resolution function, of a WAVES device with 450 blades (the largest number of blades deemed feasible in consultation with the vendor). The WAVES device inner diameter of 220 mm and outer diameter of 400 mm are constrained by both the requirement of a short secondary flight path (as described in Sec. II A) and the stress/strain limitations at 17 000 rpm of the rotor material (a high stress aluminum alloy) and the blade material (boron-loaded

carbon fiber reinforced polymer). The calculations have been performed for both the infinitely thin blades and 0.48 mm thick blades. The blade curvature for these calculations was set to transmit neutrons with $v_f = 197.8$ m/s in the horizontal plane of the sample, which, for neutrons scattered by the sample with a total velocity of 272.8 m/s ($\lambda_f = 14.50$ Å), corresponds to a vertical scattering angle component of 43.5° . The main goal of the calculation was to investigate the effect of the diameter of an annular sample on the transmission (resolution) of the WAVES device. The sample in the calculation was a 5 mm tall, thin wall cylinder with a variable diameter, d .

The benchmark calculations for the two-dimensional scattering geometry ($\alpha = 0^\circ$), as presented in the top panels of Fig. 4, demonstrate that a finite blade thickness reduces the peak transmission of unity, which is achieved with infinitely thin blades and a point sample ($d = 0$) for neutrons with 197.8 m/s velocity, in accordance with the analytical expression. A reduction in the peak transmission for the 0.48 mm thick blades compared to the infinitely thin blades is observed universally for all the configurations presented in Fig. 4. For neutrons scattered within a narrow range of the vertical scattering angle component ($29.9^\circ < \alpha < 30.1^\circ$), the transmission function remains essentially the same, except for the shift of the peak transmission from 197.8 m/s to $(197.8 \text{ m/s}) / \cos 30^\circ = 228.4$ m/s. However, for neutrons detected over a wider spread of the vertical scattering angle component ($29^\circ < \alpha < 31^\circ$), the peak transmission significantly decreases, and the transmission function becomes broader. Similar transmission functions are observed for $34^\circ < \alpha < 36^\circ$ and $39^\circ < \alpha < 41^\circ$, except for the shift of the peak transmission to $(197.8 \text{ m/s}) / \cos 35^\circ = 241.4$ m/s and $(197.8 \text{ m/s}) / \cos 40^\circ = 258.2$ m/s, respectively. These results demonstrate that for maintaining the energy resolution of a WAVES device at the BWAVES spectrometer it is imperative to use linear (vertical) position-sensitive detectors and perform data reduction separately for each pixel height (i.e., the vertical scattering angle component), and then combine the detector height-specific datasets. Such detector height-specific data reduction approach will also account for the variation in the TOF over the secondary flight path between the sample and the detector pixels. This is somewhat analogous to the data reduction approach that has to be employed at the BASIS spectrometer to achieve the highest energy resolution,⁷ where both the secondary flight path and the crystal analyzer Bragg angle depend somewhat on the vertical component of the scattering angle.

Besides this conclusion, the major observation taken from the data in Fig. 4 is a strong effect of the sample size on the WAVES transmission function. It is obvious that an increase in the sample diameter beyond ~ 5 mm leads to the pronounced deterioration of the transmission function and a visible split of the transmission peak. Therefore, a small sample size is imperative for a spectrometer that utilizes a WAVES device, such as BWAVES. This consideration based on the sample size dependence of the transmission function applies to the sample height and, due to the cylindrical symmetry of a WAVES device, would apply equally to the sample width and thickness, except that the practical restrictions on the sample thickness are much more stringent regardless. They are driven by reducing the effects of multiple scattering in the sample and necessitate the use of either thin annular (as opposed to cylindrical) or thin flat plates samples. For example, to achieve a customary acceptable value of no less than $\sim 90\%$ neutron transmission through a water sample, a

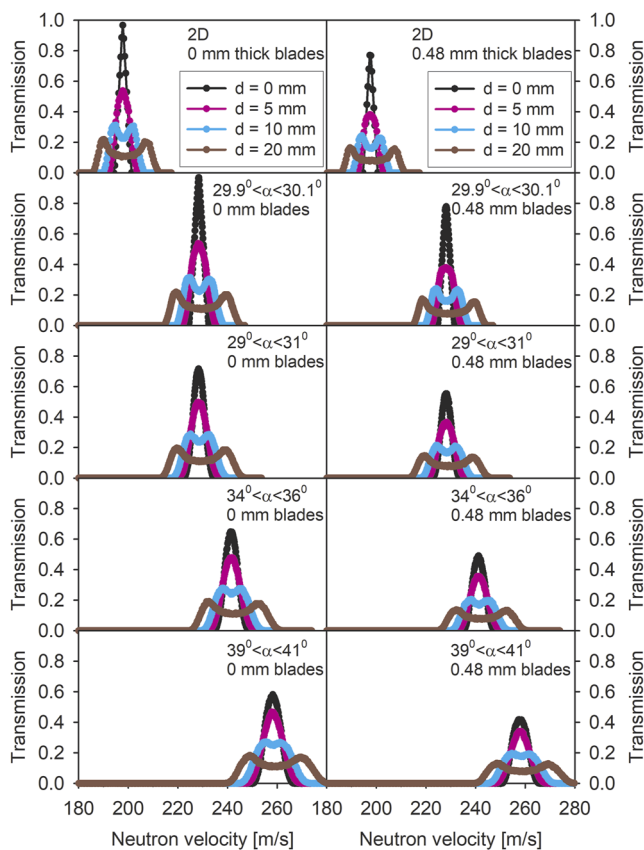


FIG. 4. Transmission function of the WAVES device with 450 blades (either infinitely thin, or 0.48 mm thick), an inner diameter of 220 mm, an outer diameter of 400 mm, spinning at 283.3 Hz (17 000 rpm), as a function of an annular sample diameter, d . The blades curvature is designed for transmission of neutrons with $v_f = 197.8$ m/s in the horizontal plane of the sample. This corresponds to the standard operation mode of BWAVES with $\lambda_f = \lambda_{\text{elastic}} = 14.50$ Å.

0.05 mm thick annulus or a 0.10 mm thick flat plate would be needed with any spectrometers, while BWAVES further restricts the sample height and width to no more than 5 mm.

D. Other components and spectrometer vacuum detector vessel

Figure 5 shows the BWAVES vacuum detector vessel with the principal components identified. The top flange of the vacuum detector vessel features recessed sectors in the direction of the incoming and outgoing neutron beam to allow unobstructed propagation of the beam with a vertical and horizontal divergence of 1.5° to the sample position and beyond. The sample's vertical position is thus within the depth of the recessed sectors. Narrower and shallower recessed sectors at various angles with respect to the incident beam are to allow sample illumination by optional laser beams when permitted by the optically transparent sample environment equipment. The use of such equipment, while optional, is enabled by the requirement of having an open tabletop geometry, as necessitated by utilization of WAVES device. The sample's horizontal position is centered over the inverted top head depression in the vessel designed to accommodate sample environment equipment, such as closed cycle refrigerators, cryostats, etc., suspended from the above. Neutrons scattered by the sample into the bottom hemisphere need to pass first through the spinning WAVES rotor. Because WAVES rotors filter out neutron velocities, but not necessarily the neutrons scattered at the off-centered positions, a stationary radial collimator with straight vertical blades surrounds the rotating WAVES. Preliminary calculations suggest that, because of the narrow depth of the collimator, with the differential between its external and internal radii not exceeding 0.05 m, between 360 and 720 vertical blades (a collimation between 1.0° and 0.5°) may be required to efficiently filter out the parasitic scattering originating at distances just beyond 2.5 mm from the WAVES device vertical axis. In turn, the collimator is surrounded by a cylindrical array of vertical linear position-sensitive neutron detector tubes, so that, besides the energy transfer, $E = E_i - E_f$, the momentum transfer, $Q = [k_i^2 + k_f^2 - 2k_i k_f \cos(2\theta)]^{1/2}$ can be calculated pixel-by-pixel.

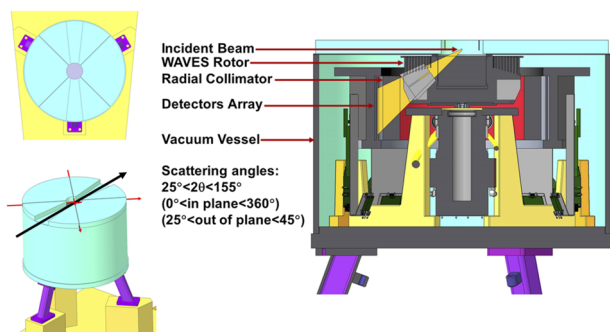


FIG. 5. Left: top view (top) and perspective view (bottom) of the BWAVES vacuum detector vessel. The neutron beam passing through the sample is shown by the bold black arrow. Optional laser beams passing through the sample positions are shown by red arrows. Right: the BWAVES vacuum detector vessel cross section and the principal spectrometer components. The external diameter of the BWAVES vacuum vessel is ~ 1 m.

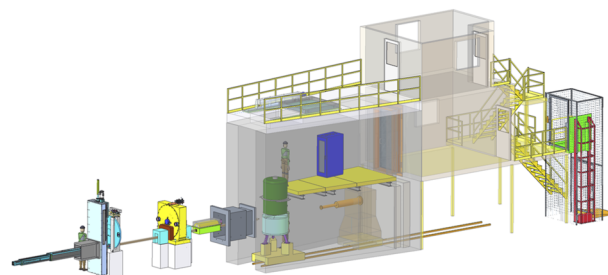


FIG. 6. Overall layout of the BWAVES beamline; the view with the neutron source (moderator, not shown) on the left. Components inside the bunker: upstream part of the guide (gray/blue), bandwidth disk chopper positioned at 6 m from the moderator (blue), T0 chopper positioned at 9.25 m from the moderator (yellow), and shutter (brown/light green). Components outside the bunker: spectrometer vacuum vessel centered at 14.65 m from the moderator (light blue), sample environment equipment suspended from above the vessel (green), and "get lost" tube (orange). The external diameter of the BWAVES vessel (light blue-colored) cylinder is ~ 1 m.

The rotor's motor, structural elements, detectors' electronics, and assorted pieces of neutron shielding also occupy the vessel's space, sharing its vacuum with the aforementioned spectrometer components. The detected scattered neutrons (represented schematically by the orange trapezoid in Fig. 5) span an in-plane scattering angle range of 0° to 360° and an out-of-plane scattering angle range of 25° to 45° , resulting in a measurable range of scattering angles $25^\circ < 2\theta < 155^\circ$. With the maximum radius of the WAVES rotor of ~ 0.2 m and the radius of the detector circle of ~ 0.3 m, the diameter of the vacuum vessel can be minimized down to below 1 m, which is crucial for placement of the BWAVES spectrometer close to the bunker wall between the structures of the neighbor beam lines.

Figure 6 illustrates the overall layout of the BWAVES beamline (inside the bunker, upstream, and inside the spectrometer enclosure, downstream). Of importance to note is the three-level access to the spectrometer vessel. Components could be installed into or removed from the spectrometer enclosure through an opening in the enclosure ceiling using a crane. Access through the mezzanine, elevated somewhat above the vessel, is to be utilized, e.g., for changing samples measured using sample environment equipment. Finally, access from the floor level can be utilized for installation and manipulation of the samples that are measured under ambient or near-ambient conditions. Such samples can either be supported from the above or placed onto a small goniometer resting on the bottom of the inverted top hat depression. Optional laser sources and detectors that can be used in conjunction with the optically transparent sample environment equipment also could be serviced from the floor level. Additionally, placing the spectrometer vessel on rails may allow servicing of the vessel rolled out of the enclosure, as needed.

IV. SPECTROMETER PERFORMANCE

A. The (E, Q) space coverage, energy resolution, and count rate

Figure 7 shows the coverage in the (E, Q) space provided by the BWAVES spectrometer in single-frame operation with

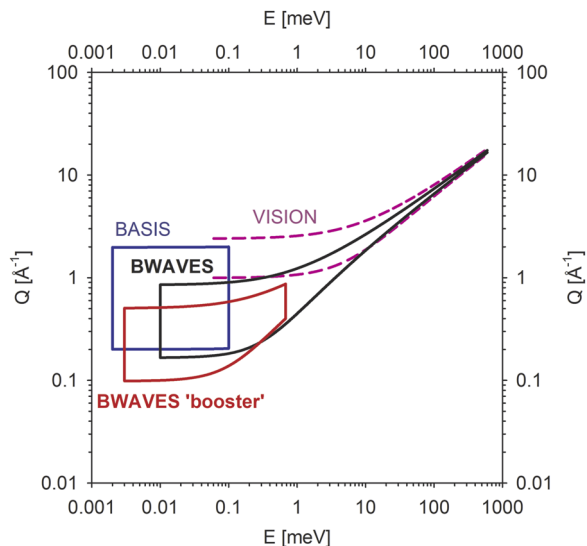


FIG. 7. The (E, Q) space coverage provided by the BWAVES spectrometer with $\lambda_f = 14.50 \text{ \AA}$ (as a single frame spectrum continuous as a function of E and Q) in comparison with the SNS FTS inverted geometry spectrometers in operation, BASIS and VISION. Also shown is an example of the BWAVES “booster” mode with an arbitrarily chosen $\lambda_f = 24.50 \text{ \AA}$, as discussed in the text.

$\lambda_f = 14.50 \text{ \AA}$. The corresponding data for the SNS First Target Station (FTS) spectrometers in operation, BASIS and VISION, are presented for comparison. As mentioned above, with analyzer banks positioned only at two scattering angles, VISION lacks continuous Q coverage, measuring scattering signal only along the two trajectories in the (E, Q) space. At high energy transfers, the VISION and BWAVES coverages largely overlap, but the latter spectrometer features continuous Q coverage at moderate and low energy transfers, bridging the gap between the vibrational (VISION) and high-resolution backscattering (BASIS) spectrometers.

The performance of the BWAVES spectrometer was evaluated using McStas^{16,17} and MCViNE^{18,19} packages. Figure 8 shows the incident neutron flux at BWAVES for a $5 \times 5 \text{ mm}^2$ spot at the sample position. The total wavelength-integrated flux at the BWAVES sample position is $\sim 1 \times 10^9$ neutron/(cm^2/s). For comparison, the incident flux on the IRIS spectrometer with an energy resolution similar to that of BWAVES was reported as 1×10^7 neutron/(cm^2/s) for the white beam at the full source intensity.^{3,4} However, one needs to take into consideration the difference in the sample size: $\sim 0.25 \text{ cm}^2$ for BWAVES vs $\sim 6.7 \text{ cm}^2$ for IRIS, which results in the more comparable flux over the actual sample: 2.5×10^8 neutron/s on BWAVES vs 0.67×10^8 neutron/s on IRIS. That is, the main difference is in the extent of the beam focusing rather than the total flux on the sample. The effect of the guide transmission cutoff is evident at wavelengths shorter than $\sim 2.5 \text{ \AA}$, similar to the brilliance transfer data presented in Fig. 3.

As the BWAVES spectrometer is designed for a reasonably high energy resolution, the important parameters to test using the full McStas/MCViNE model of the spectrometer are the BWAVES resolution function and its collection rate using standard samples.

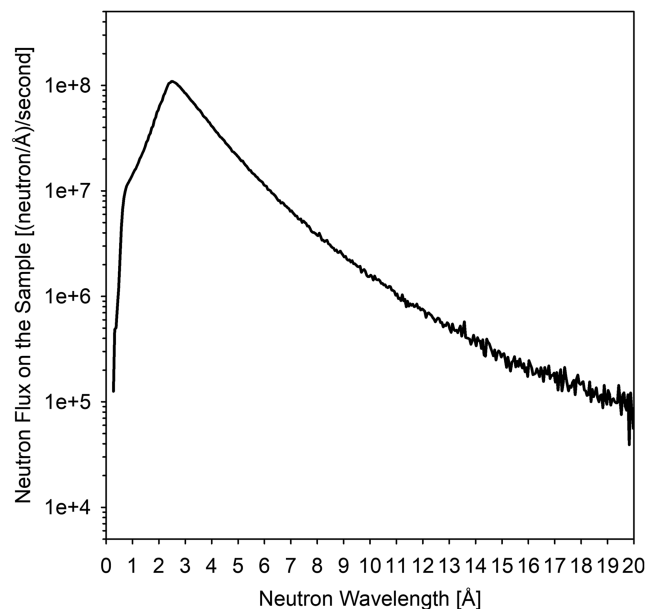


FIG. 8. The incident neutron flux calculated for the BWAVES spectrometer for a $5 \times 5 \text{ mm}^2$ spot at the sample position.

The results are presented in Fig. 9 for a cylindrical sample, 5 mm in height and 5 mm in diameter, with the neutron scattering cross section (completely incoherent) of 0.2 cm^{-1} , that is, a 10% incoherent scatterer with the BWAVES design sample geometry. The resolution function, summed over all detectors, is highly Gaussian in shape, with a FWHM of 0.018 meV. For a 10% incoherent scatterer, it is collected at a rate of 2400 counts per second. One of the insets in Fig. 9 presents the spectrum collected from this sample in 1 s.

Moreover, the energy resolution of BWAVES could be adjusted (improved), at the expense of the reduced range of the high energy transfers, using an optional “booster” mode, when a reduced rotation frequency of the WAVES rotor results in transmission and detection of the lower velocity (longer wavelength) neutrons. The incident chopper transmission bandwidth is then shifted to ensure the measurement of the elastic line with the new (longer) λ_f , which is associated with the higher energy resolution. An example of the “booster” mode presented in Fig. 7 illustrates the (E, Q) space coverage attainable with an arbitrarily chosen $\lambda_f = 24.50 \text{ \AA}$. Because the WAVES velocity can be reduced in a continuous fashion, the (E, Q) space coverage and the associated energy resolution at the elastic line could be adjusted as desired. An example of the signal measured in the “booster” operation as obtained from McStas/MCViNE model of the spectrometer is presented in Fig. 10 for the same 10% incoherent scatterer with the BWAVES design sample geometry as used for the regular BWAVES operation (Fig. 9). With $\lambda_f = 24.50 \text{ \AA}$, the $1/\lambda_f^2$ scaling law predicts a FWHM of 0.006 meV, which is indeed achieved in the McStas/MCViNE model; the resolution function is still highly Gaussian. The “booster” mode count rate at the elastic line with $\lambda_f = 24.50 \text{ \AA}$ is 5–6 times lower compared to the regular BWAVES operation mode with $\lambda_f = 14.50 \text{ \AA}$.

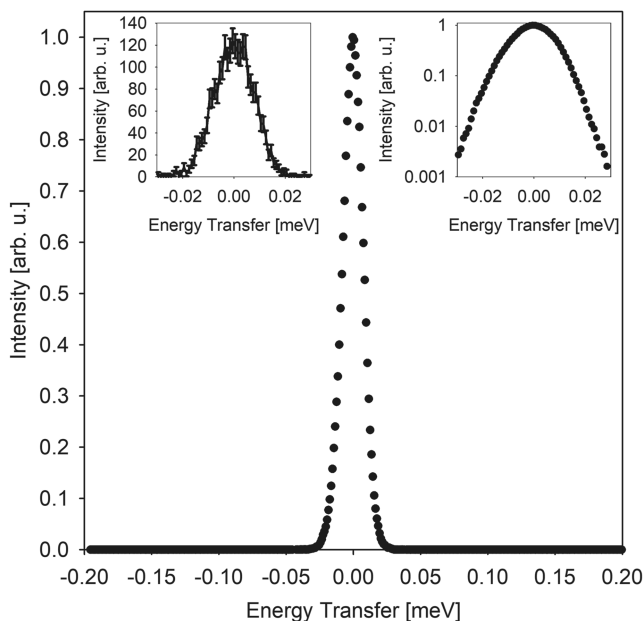


FIG. 9. BWAVES resolution function (peak intensity normalized to unity) calculated from the full McStas/MCViNE model of the instrument. Right inset: logarithmic scale intensity. Left inset: the data from the same sample (a 10% incoherent scatterer) collected in 1 s. The ± 0.20 meV range is shown for clarity and does not represent the actual, much broader, range of energy transfers accessible in the standard operation mode of BWAVES.

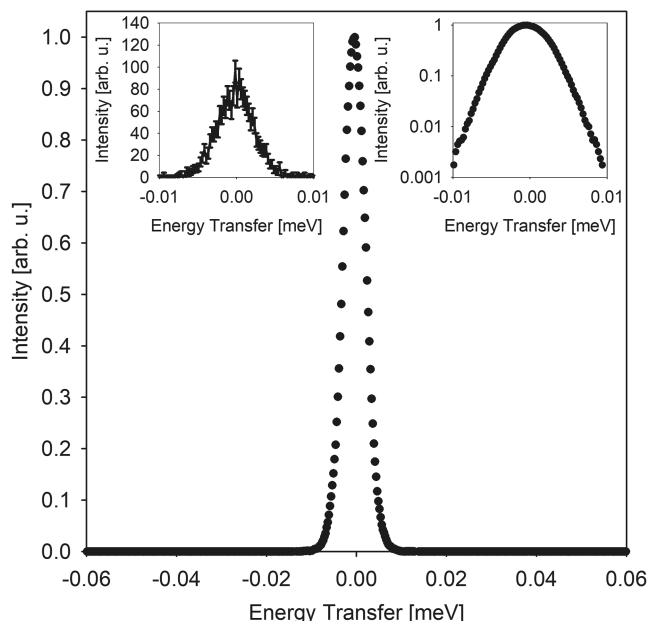


FIG. 10. BWAVES resolution function (peak intensity normalized to unity) for a "booster" operation mode with $\lambda_f = 24.50$ Å calculated from the full McStas/MCViNE model of the instrument. Right inset: logarithmic scale intensity. Left inset: the data from the same sample (a 10% incoherent scatterer) collected in 5 s. The ± 0.06 meV range is shown for clarity and does not represent the actual, much broader, range of energy transfers accessible in the "booster" operation mode of BWAVES.

B. A virtual experiment at the BWAVES spectrometer

Using the full McStas/MCViNE model of BWAVES in the standard operation mode with $\lambda_f = 14.50$ Å and the incident bandwidth from 0.23 to 17.44 Å, we have performed a virtual neutron scattering experiment with a powder sample of a molecular antiviral drug, apilimod ($C_{23}H_{26}N_6O_2$, CAS 541550-19-0), loaded in a cylindrical sample holder, 5 mm in height and 5 mm in diameter, with the packing density to give the total incoherent scattering cross section for the sample of 0.2 cm^{-1} (that is, a 10% incoherent scatterer with the BWAVES design sample geometry). Apilimod was chosen for the virtual experiment because of our very recent extensive computational and experimental investigation of both vibrational and relaxational dynamics in this molecular drug. Apilimod is an interleukin- and lipid kinase enzyme-inhibitor with demonstrated efficacy against Ebola, Lassa, and Marburg viruses^{20,21} and, more recently, *in vitro* efficacy against SARS-CoV-2 virus.^{22,23} Although the primary action mechanism of molecular drug compounds is usually drug-specific, on the fundamental level, the effectiveness of the formation of the ligand-receptor complex between the target receptor and the drug (ligand) is ultimately governed by the biomolecular thermodynamics. To attain a thermodynamically favorable reaction state, biochemical reactions usually need to be catalyzed. At the molecular level, the small-amplitude atomic motions enable efficient exploration of the configurational states of the energy landscape²⁴ to sample the potentially thermodynamically favorable reaction states. Among such motions, methyl group rotations are particularly important because of the relative ease of thermal activation.²⁵

The model scattering function, $S(Q, E)$, input for the simulation of the scattering kernel by the apilimod sample was constructed on the basis of the simulation results from a neutron scattering study of dynamics in apilimod²⁶ aimed at comparison with a neutron scattering study of dynamics in a benchmark antiviral drug, remdesivir.²⁷ From the standpoint of a QENS experiment, it is most beneficial to allocate more time to the measurement at the baseline temperature. This is because such a measurement is often used in the data fitting to be numerically convolved with the model scattering function for the data collected at all other temperatures. Therefore, the improved counting statistics for a single baseline run benefits the largest number of datasets to be fitted. Thus, the apilimod data at 10 K collected (virtually) for a relatively long time of 5 h are presented in Fig. 11.

As one can see in Fig. 11, the vibrational part of the apilimod spectrum at 10 K is well defined and separated from the low-energy part by a gap (consistent with the model $S(Q, E)$ at this baseline temperature, with no measurable QENS signal). Besides the elastic line, there is a well-defined peak at 0.080 meV. The data plotted on the linear scale of the energy transfer shows that this peak appears on both the neutron energy loss and energy gain sides, at ± 0.080 meV. Furthermore, the position of these peaks is independent of Q , characteristic of quantum tunneling. Thus, this virtual measurement identifies the methyl rotation quantum tunneling peaks for the group with the rotational barrier height of 15 meV. No tunneling peaks are visible in this measurement that could be associated with the other methyl group in the apilimod crystal structure, with a rotational barrier height of 32 meV.

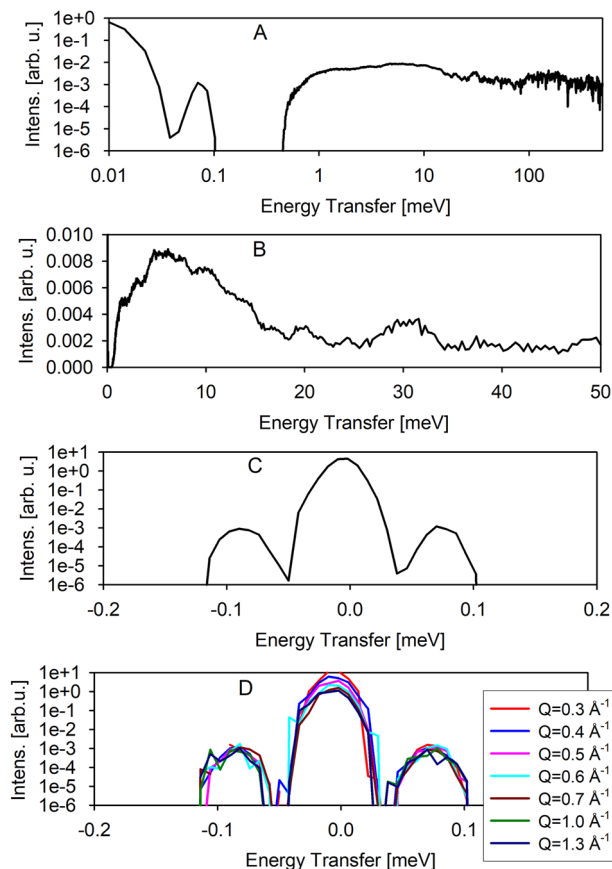


FIG. 11. Apilimod at 10 K, measured at the BWAVES spectrometer (virtually) for 5 h. Panels from top to the bottom. (a) The data summed over all detectors plotted over the entire accessible energy transfer range. (b) The data summed over all detectors zoomed in to show the lower-energy INS part of the spectrum. (c) The data summed over all detectors zoomed in to show the low-energy QENS part of the spectrum. The methyl quantum tunneling peaks at ± 0.080 meV are evident. (d) Same as above but plotted in the Q -resolved mode. The peaks position is independent of Q , as expected for the tunneling modes.

The 40 K apilimod data collected (virtually) for 2.5 h (Fig. 12) show an INS spectrum quite similar to that observed at 10 K, but with increased intensity, characteristic of vibrational modes. The quantum tunneling peak at 0.080 meV had disappeared, but there is no longer a gap separating the INS part of the spectrum from the low-energy part. Instead, there seems to be QENS signal filling this gap. Furthermore, it appears that this signal might have two components, and the position of both of them may be independent of Q , indicative of stochastic rotational jumps of methyl groups over the potential barriers.

The 310 K apilimod data collected (virtually) for 2.5 h (Fig. 13) show further increase in the intensity of the vibrational modes at intermediate energy transfers, even while the data at high energy transfers (above ~ 100 meV) become strongly damped due to the exponential decay of the Debye–Waller vibrational thermal factors. The QENS spectrum has grown in intensity and clearly demonstrates the presence of two components, with their positions still

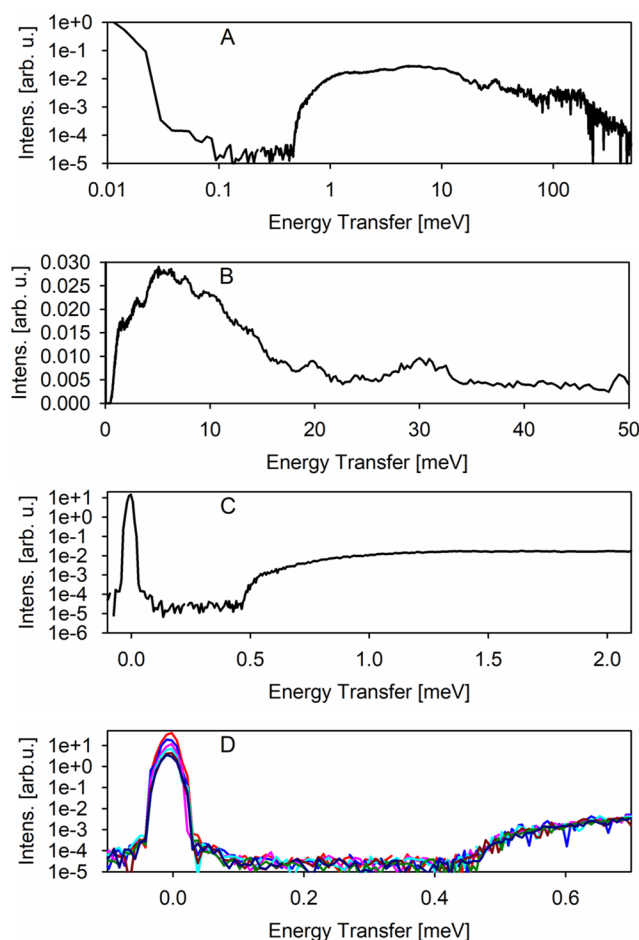


FIG. 12. Apilimod at 40 K, measured at the BWAVES spectrometer (virtually) for 2.5 h. Panels from top to the bottom. (a) The data summed over all detectors plotted over the entire accessible energy transfer range. (b) The data summed over all detectors zoomed in to show the lower-energy INS part of the spectrum. (c) The data summed over all detectors zoomed in to show the extended QENS part of the spectrum and the beginning of the INS part of the spectrum. (d) Same as above but plotted in the Q -resolved mode and further zoomed in. The development of the QENS components is now evident. They appear to be independent of Q , as expected for the methyl stochastic jumps. The designation of the Q values by color is the same as was used in the bottom panel of Fig. 11.

independent of Q , due to the stochastic methyl jumps over the potential barriers. Thus, the BWAVES measurements reveal the development of the two QENS components, which are already visible in the data collected at 40 K.

Since these components are associated with the two methyl groups in different environments in the apilimod crystal structure, in principle, another quantum tunneling peak, associated with the rotational barrier height of 32 meV, should be present in the scattering spectrum at an energy transfer lower than 0.080 meV. In practice, however, such tunneling peaks may be buried deep within the resolution line. Nevertheless, the actual measurements on VISION vibrational spectrometer²⁶ (and the virtual measurements on BWAVES) indeed show the methyl librational modes

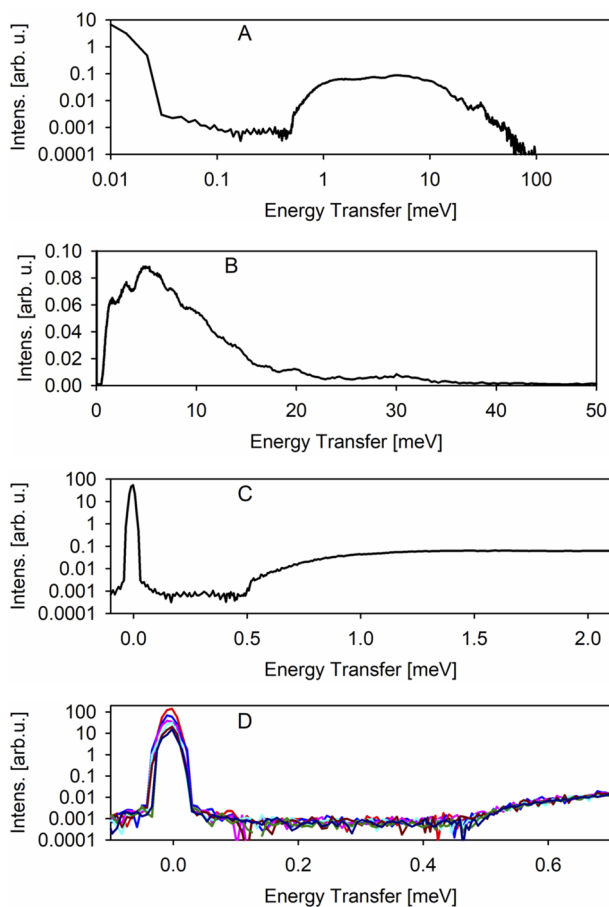


FIG. 13. Apilimod at 310 K, measured at the BWAVES spectrometer (virtually) for 2.5 h. Panels from top to the bottom. (a) The data summed over all detectors plotted over the entire accessible energy transfer range. (b) The data summed over all detectors zoomed in to show the lower-energy INS part of the spectrum. (c) The data summed over all detectors zoomed in to show the extended QENS part of the spectrum and the beginning of the INS part of the spectrum. (d) Same as above but plotted in the Q-resolved mode and further zoomed in. The growth of the QENS components is now evident. They appear to be independent of Q , as expected for the methyl stochastic jumps. The designation of the Q values by color is the same as was used in the bottom panel of Fig. 11.

consistent not only with the 15 meV rotational barrier giving rise to the observed at ± 0.080 meV tunneling peaks but also the 32 meV rotational barrier that should be giving rise to the tunneling peaks ± 0.008 meV. That is, the actual observation of the librational modes at BWAVES would have suggested to look for the tunneling peaks ± 0.008 meV, possibly buried within the BWAVES resolution line in the standard operation mode. Indeed, the McStas/MCViNE model shows that these tunneling peaks could be resolved using “booster” mode with $\lambda_f = 28.50$ Å, when the BWAVES energy resolution reaches FWHM of ~ 0.004 meV (Fig. 14). However, the counting statistics become low under these conditions (significantly lower even compared to the data collected with $\lambda_f = 24.50$ Å to reach a FWHM of 0.006 meV from a 10% scattering sample as presented in Fig. 10). Thus, attaining such a fine energy resolution in

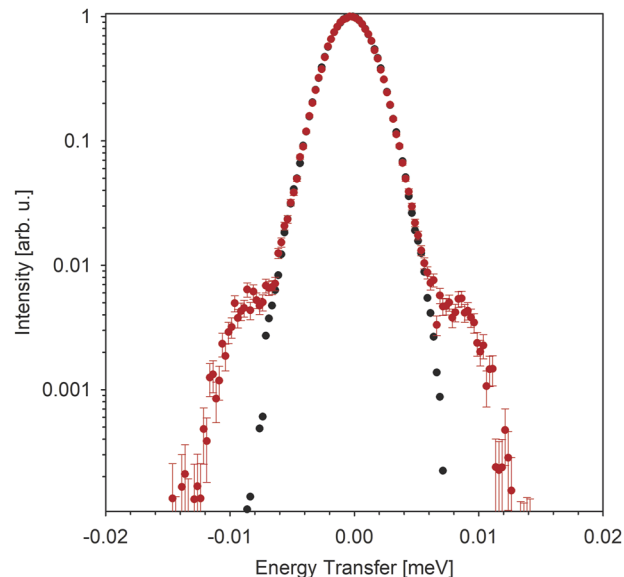


FIG. 14. BWAVES resolution function (black) and the apilimod (red) measured at BWAVES in the “booster” mode (virtually) with $\lambda_f = 28.50$ Å for 48 h. The quantum tunneling peaks at ± 0.008 meV become resolved.

practical operation should be considered only borderline feasible. This example illustrates that, while there is no hard limit cutoff for the energy resolution attainable in the “booster” mode, striving for the highest energy resolution may become impractical from the viewpoint of the experiment duration. For even higher rotational energy barriers, resolving the quantum tunneling peaks would become outright impossible. However, even in such case, the broad dynamic range of the BWAVES spectrometer is indispensable for capturing, simultaneously, the QENS components originating from the stochastic jumps of all the methyl groups, once they become sufficiently broad upon increasing the temperature. The strength specific to the inverted geometry spectrometers, such as BWAVES, is their ability to access the entire energy transfer range at any measurement temperature (on the neutron energy loss side). Therefore, accurate temperature evolution of the tunneling vs quasielastic and vs low vibrational modes can be assessed simultaneously. Besides, explorational use of the “booster” mode in search of the expected low-lying quantum tunneling excitations may be suggested by observation and analysis of the librational modes.

C. Final remarks on the BWAVES spectrometer capabilities

The BWAVES dynamic range of measurable energy transfers spanning 4.5 decades is a new capability in high energy-resolution neutron spectroscopy. As usual, the introduction of a new capability will enable new science while likely necessitating new approaches to the data analysis. For example, the introduction of the BASIS spectrometer⁷ combining a high energy resolution and a sufficiently broad (for a backscattering spectrometer) accessible range of energy transfers led to the development of a new *Ansatz* describing the two-component QENS signal originated from the localized and

long-range translational motion of single species. While originally developed and applied to describe QENS from fluids,²⁸ conceptually similar *Ansätze* linking the localized and long-range translational motions of single species have been broadly applied to a range of systems measured at BASIS, e.g., lipids in membranes.²⁹ The presence of the third QENS components in the scattering spectra collected at BASIS can sometimes be inferred,²⁸ but explicit fits of BASIS data with three QENS components have been rare and beset with difficulties.^{30,31} This presents a problem for studying relaxational dynamics of biomolecules, such as proteins,³² which customarily requires taking measurements at several different neutron spectrometers.³³ The use of several spectrometers is a very time and sample consuming process that requires arbitrary matching of the data obtained on different spectrometers, often with different *Q* ranges, thus precluding analysis of the geometry of molecular motion over the full energy (time) range. BWAVES, due to its uniquely broad dynamic range, will resolve this long-standing problem.

V. CONCLUSION

We anticipate that BWAVES will become a highly sought-after spectrometer with a broad user base. Some of the scientific challenges that BWAVES will be able to address using its unique capabilities, such as the aforementioned broad multi-component dynamic analysis in complex systems, are evident at present, while others will undoubtedly be identified in the course of the spectrometer lifetime. The following characteristics are expected to set BWAVES apart from other inverted geometry neutron spectrometers:

- (1) As a truly broadband neutron scattering spectrometer, with an unmatched dynamic range spanning 4.5 decades and covering energy transfers from below 0.010 meV to above 500 meV, BWAVES is expected to have a transformative impact benefiting research in soft and biological materials and chemical and materials sciences.
- (2) As the only inverted geometry spectrometer currently proposed for SNS STS, BWAVES could be uniquely suited to map relaxational excitations gradually emerging as a function of temperature, or other thermodynamic variables, thereby efficiently deciphering complex dynamic landscapes.
- (3) Thanks to its small beam size, BWAVES may enable studies of very small samples (a few microliters in volume) and facilitate the use of small-volume size advanced sample environment equipment.
- (4) As an open-tabletop sample geometry instrument, unique among the high-energy resolution and vibrational neutron spectrometers worldwide, BWAVES may provide easy access to the sample position for application of multimodal external stimuli, including default optical access to the sample.
- (5) BWAVES is expected to serve as the gateway (and oftentimes the one-stop) spectrometer for neutron scattering studies of dynamics in the broadest range of materials, in the same manner as SANS and ND instruments serve as the gateway for structural studies.

To ensure a near perfect match of the BWAVES spectrometer to the STS capabilities, the BWAVES design utilizes several unique technical solutions, the central among them being a novel WAVES rotor. Furthermore, BWAVES benefits from a set of the intertwined

source characteristics of the STS (frequency, cold neutrons, high brightness, and compact moderators). BWAVES will be highly beneficial for (bio)materials and chemical science for the development of fundamental understanding of materials for energy applications, novel recyclable polymers, and for a deep understanding of biological processes critical for emerging bio- and medical technologies. These advances in neutron scattering are expected to greatly benefit and broaden the user community.

ACKNOWLEDGMENTS

The design of BWAVES has been the result of efforts by many contributors. This research used resources of the Spallation Neutron Source Second Target Station Project at Oak Ridge National Laboratory (ORNL). ORNL is managed by UT-Battelle LLC for DOE's Office of Science, the single largest supporter of basic research in the physical sciences in the United States. The operation and user program at the Spallation Neutron Source is supported by the Scientific User Facilities Division, Office of Basic Energy Sciences, U.S. Department of Energy. This article has been authored by UT-Battelle, LLC, under Contract No. DE-AC05-00OR22725 with the U.S. Department of Energy (DOE). The U.S. government retains and the publisher, by accepting the article for publication, acknowledges that the U.S. government retains a nonexclusive, paid-up, irrevocable, worldwide license to publish or reproduce the published form of this manuscript, or allow others to do so, for U.S. government purposes. DOE will provide public access to these results of federally sponsored research in accordance with the DOE Public Access Plan (<http://energy.gov/downloads/doe-public-access-plan>).

AUTHOR DECLARATIONS

Conflict of Interest

The authors have no conflict to disclose.

Author Contributions

E.M. initiated and developed the concept and the project, participated in the discussion and analysis at all stages of the projects, and wrote the paper together with all co-authors. C.B. was involved in the conceptual design and provided Creo support for the proposal. M.J.F. was involved in the concept and simulation development. K.W.H. was engaged in the conceptual design discussions and provided initial calculations of neutron flux estimates. T.H. performed the guide simulations in McStas. J.L. performed simulation and analysis for the WAVES device and carried out virtual experiments for evaluating spectrometer performance, including the resolution and virtual samples. B.M. was involved in the CAD design/modeling of the concept. W.M. was involved with the conceptual design of the WAVES rotor and rotor vacuum chamber for the instrument. A.D.S. performed the guide simulations in McStas and was involved in the concept and simulation development. P.T. was involved with the engineering development of the concept. W.T. provided design insight and assisted in the development of the CAD model. All co-authors contributed to the paper.

DATA AVAILABILITY

The data that support the findings of this study are available from the corresponding author upon reasonable request.

REFERENCES

- ¹A. Meyer, R. M. Dimeo, P. M. Gehring, and D. A. Neumann, *Rev. Sci. Instrum.* **74**, 2759–2777 (2003).
- ²J. Wuttke, A. Budwig, M. Drochner, H. Kämmerling, F.-J. Kayser, H. Kleines, V. Ossovyi, L. C. Pardo, M. Prager, D. Richter, G. J. Schneider, H. Schneider, and S. Staringer, *Rev. Sci. Instrum.* **83**, 075109 (2012).
- ³C. J. Carlile and M. A. Adams, *Physica B* **182**, 431–440 (1992).
- ⁴M. T. F. Telling, S. I. Campbell, D. D. Abley, D. A. Cragg, J. J. P. Balchin, and C. J. Carlile, *Appl. Phys. A: Mater. Sci. Process.* **74**, s61–s63 (2002).
- ⁵M. T. F. Telling and K. H. Andersen, *Phys. Chem. Chem. Phys.* **7**, 1255–1261 (2005).
- ⁶B. Frick, E. Mamontov, L. van Eijck, and T. Seydel, *Z. Phys. Chem.* **224**, 33–60 (2010).
- ⁷E. Mamontov and K. W. Herwig, *Rev. Sci. Instrum.* **82**, 085109 (2011).
- ⁸K. Shibata, N. Takahashi, Y. Kawakita, M. Matsuura, T. Yamada, T. Tominaga, W. Kambara, M. Kobayashi, Y. Inamura, T. Nakatani, K. Nakajima, and M. Arai, *JPS Conf. Proc.* **8**, 036022 (2015).
- ⁹M. Appel, B. Frick, and A. Magerl, *Physica B* **562**, 6–8 (2019).
- ¹⁰D. Colognesi, M. Celli, F. Cilloco, R. J. Newport, S. F. Parker, V. Rossi-Albertini, F. Sacchetti, J. Tomkinson, and M. Zoppi, *Appl. Phys. A: Mater. Sci. Process.* **74**, S64–S66 (2002).
- ¹¹P. A. Seeger, L. L. Daemen, and J. Z. Larese, *Nucl. Instrum. Methods Phys. Res., Sect. A* **604**, 719–728 (2009).
- ¹²E. Mamontov, *Nucl. Instrum. Methods Phys. Res., Sect. A* **759**, 83–91 (2014).
- ¹³E. Mamontov, *J. Neutron Res.* **18**, 21–28 (2015).
- ¹⁴E. Mamontov, *J. Phys.: Condens. Matter* **28**, 345201 (2016).
- ¹⁵S. Magazù and E. Mamontov, *Biochim. Biophys. Acta* **1861**, 3632–3637 (2017).
- ¹⁶P. K. Willendrup and K. Lefmann, *J. Neutron Res.* **22**, 1–16 (2020).
- ¹⁷P. K. Willendrup and K. Lefmann, *J. Neutron Res.* **23**, 7–27 (2021).
- ¹⁸J. Y. Y. Lin, H. L. Smith, G. E. Granroth, D. L. Abernathy, M. D. Lumsden, B. Winn, A. A. Aczel, M. Aivazis, and B. Fultz, *Nucl. Instrum. Methods Phys. Res., Sect. A* **810**, 86–99 (2016).
- ¹⁹J. Y. Y. Lin, F. Islam, G. Sala, I. Lumsden, H. Smith, M. Doucet, M. B. Stone, D. L. Abernathy, G. Ehlers, J. F. Ankner, and G. E. Granroth, *J. Phys. Commun.* **3**, 085005 (2019).
- ²⁰E. A. Nelson, J. Dyall, T. Hoenen, A. B. Barnes, H. Zhou, J. Y. Liang, J. Michelotti, W. H. Dewey, L. E. DeWald, R. S. Bennett *et al.*, *PLoS Neglected Trop. Dis.* **11**, e0005540 (2017).
- ²¹S. Qiu, A. Leung, Y. Bo, R. A. Kozak, S. P. Anand, C. Warkentin, F. D. R. Salambanga, J. Cui, G. Kobinger, D. Kobasa *et al.*, *Virology* **513**, 17–28 (2018).
- ²²L. Riva, S. Yuan, X. Yin, L. Martin-Sancho, N. Matsunaga, L. Pache, S. Burgstaller-Muehlbacher, P. D. De Jesus, P. Teriete, M. V. Hull *et al.*, *Nature* **586**, 113–119 (2020).
- ²³Y.-L. Kang, Y.-Y. Chou, P. W. Rothlauf, Z. Liu, T. K. Soh, D. Cureton, J. B. Case, R. E. Chen, M. S. Diamond, S. P. J. Whelan *et al.*, *Proc. Natl. Acad. Sci. U. S. A.* **117**, 20803–20813 (2020).
- ²⁴H. Frauenfelder, G. Chen, J. Berendzen, P. W. Fenimore, H. Jansson, B. H. McMahon, I. R. Stroe, J. Swenson, and R. D. Young, *Proc. Natl. Acad. Sci. U. S. A.* **106**, 5129–5134 (2009).
- ²⁵J. D. Nickels, J. E. Curtis, H. O'Neill, and A. P. Sokolov, *J. Biol. Phys.* **38**, 497–505 (2012).
- ²⁶E. Mamontov, Y. Cheng, L. L. Daemen, A. I. Kolesnikov, A. J. Ramirez-Cuesta, M. R. Ryder, and M. B. Stone, *Chem. Phys. Lett.* **777**, 138727 (2021).
- ²⁷E. Mamontov, Y. Cheng, L. L. Daemen, A. I. Kolesnikov, A. J. Ramirez-Cuesta, M. R. Ryder, and M. B. Stone, *J. Phys. Chem. Lett.* **11**, 10256–10261 (2020).
- ²⁸E. Mamontov, H. Luo, and S. Dai, *J. Phys. Chem. B* **113**, 159–169 (2009).
- ²⁹V. K. Sharma, E. Mamontov, D. B. Anunciado, H. O'Neill, and V. Urban, *J. Phys. Chem. B* **119**, 4460–4470 (2015).
- ³⁰D. V. Wagle, G. A. Baker, and E. Mamontov, *J. Phys. Chem. Lett.* **6**, 2924–2928 (2015).
- ³¹C. Z. Xie, S. M. Chang, E. Mamontov, L. R. Stingaciu, and Y. F. Chen, *Phys. Rev. E* **101**, 012416 (2020).
- ³²L. Hong, N. Smolin, B. Lindner, A. P. Sokolov, and J. C. Smith, *Phys. Rev. Lett.* **107**, 148102 (2011).
- ³³S. Khodadadi and A. P. Sokolov, *Soft Matter* **11**, 4984–4998 (2015).